Moment-Curvature Analysis of R/C Jacketed Rectangular Sections Including Interface Slip Under Cyclic Loading

V.K. Papanikolaou, G.E. Thermou & A.J. Kappos
Laboratory of Reinforced Concrete and Masonry Structures
Aristotle University of Thessaloniki, Greece

SUMMARY:
The paper presents a novel computational procedure for the moment-curvature analysis of rectangular reinforced concrete (R/C) jacketed sections under cyclic loading, including the effect of potential interface slip between old and new concrete. A fiber section decomposition approach is adopted, utilizing inelastic cyclic material constitutive laws for concrete and steel, while the slipping effect is simulated by an improved cyclic interface model. Resultant internal actions are numerically integrated and the required equilibrium conditions for interface behavior are imposed. The implemented solution strategy for producing cyclic moment-curvature diagrams is based on an efficient differential evolution algorithm, showing satisfactory convergence. The performance of the suggested method is demonstrated through cyclic load analyses of jacketed R/C columns.

Keywords: R/C Jackets, Moment-Curvature Analysis, Interface Slip, Differential Evolution, Cyclic Loading

1. INTRODUCTION

Reinforced concrete (R/C) jacketing is an intervention method used extensively in practice to accommodate deficiencies related to structural response, in terms of stiffness, strength, and ductility. The application of this method leads to a uniform distribution of lateral load capacity throughout the structure and hence the enhancement of structural behavior under seismic excitation. An important aspect that plays a significant role in the structural response of jacketed members is the shear transfer efficiency along interfaces between old and new concrete. The mechanisms mobilized along interfaces due to slip and their interaction is a rather complex issue in experimental and analytical research, especially under cyclic loading conditions (notably seismic loading), where strength degradation should also be accounted for. Mechanisms that resist interface sliding are aggregate interlock between contact surfaces, including any initial adhesion of the jacket concrete on the substrate, friction owing to clamping action of reinforcement normal to the interface and dowel action of any properly anchored reinforcement crossing the sliding plane.

For the analysis of jacketed R/C member response under cyclic loading including the effect of potential interface slip, a novel computational procedure is presented herein. Section analysis is performed in moment-curvature response terms, using a fiber section decomposition approach. Inelastic cyclic material constitutive laws for concrete and steel are utilized, while the slipping effect is simulated by an improved cyclic interface model, exhibiting numerical robustness. Resultant internal actions are integrated analytically and the required equilibrium conditions for interface behavior are imposed. The implemented solution strategy for producing cyclic moment curvature diagrams is based on an efficient differential evolution algorithm, showing satisfactory convergence. Finally, the performance of the suggested method is demonstrated through cyclic moment-curvature analyses of jacketed R/C columns. In the following sections, the constitutive model formulations and the solution strategy of the present computational procedure are described in detail, and examples of the model response are provided.

2. CONSTITUTIVE MODELS

The elements required for assembling a fiber representation of a jacketed R/C section and subsequently performing cyclic moment-curvature analysis are: (a) two cyclic constitutive models for concrete and steel materials and (b) a robust cyclic interface model to simulate the slipping effect between the core (old) and jacket (new) concrete.

The constitutive model for concrete implemented in the present study is based on the uniaxial stress-strain relationship suggested by Mander et al. (1988), as adapted by Martinez-Rueda and Elnashai (1997). The confinement action due to transverse reinforcement is represented by a passive confinement factor (K), which is considered constant during loading. For the reinforcing steel, the well-known cyclic constitutive model by Menegotto and Pinto (1973) incorporating the isotropic hardening rules by Filippou et al. (1983) was implemented. The generalized response curves and the material parameters for the above constitutive models are presented in Figure 2.1 and Table 2.1, respectively. The present model implementation was validated by comparison with an established finite element software (Elnashai et al., 2010).

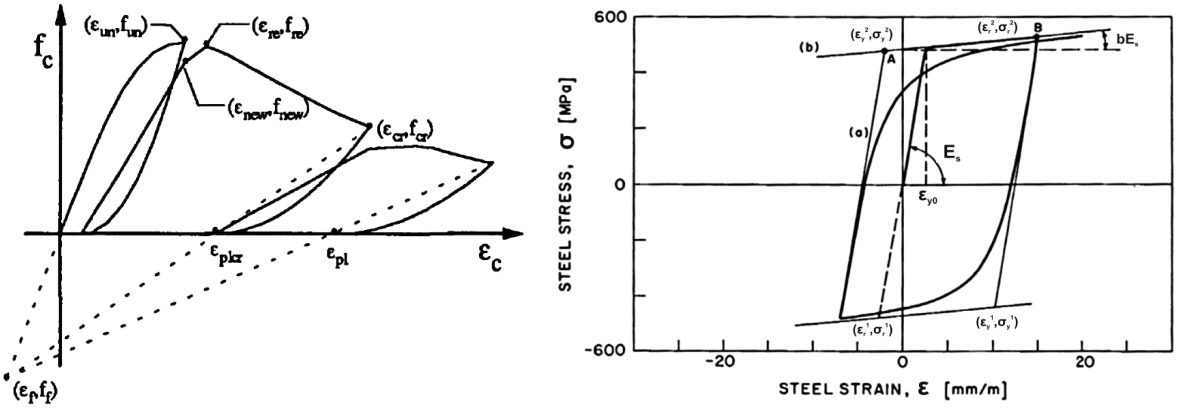

Figure 2.1. Generalized cyclic response curves for concrete (left) and steel (right) constitutive models

Table 2.1. Material constitutive model parameters (see also Fig. 2.1)

Concrete		Steel	
f_c (MPa)	Uniaxial compressive strength	E_s (MPa)	Elastic modulus
f_t (MPa)	Uniaxial tensile strength	f_y (MPa)	Yield strength
ε_{co}	Strain at maximum strength	b	Hardening factor
K	Confinement factor	R_0, A_1-A_4	Shape and isotropic hardening parameters

The interface model to be formulated in the present study should describe the shear response (V) of the core-jacket interface due to the relative slip (s) between old and new concrete, under cyclic loading. However, the available literature on this subject is extremely limited. The most relevant study by Vassilopoulou and Tassios (2003) tackles the problem of cyclic concrete-to-concrete interface modeling for the first time, yet on a limited basis, since it produces shear-slip response curves only for *symmetric* cyclic slip loading (a common situation in cyclic testing). As a result, it is attempted here to improve and extend the above formulation for arbitrarily varying cyclic loading. The interface model is based on the interaction between two distinct mechanisms: (a) dowel action of the reinforcement normal to the interface plane (b) friction forces that develop between old and new concrete (Fig. 2.2). In Table 2.2, the necessary parameters for initializing the interface model are presented.

Table 2.2. Cyclic interface model parameters

E_c (MPa)	Concrete elastic modulus	E_s (MPa)	Steel elastic modulus
f_c (MPa)	Concrete uniaxial tensile strength	f_y (MPa)	Steel yield strength
A_c (m^2)	Interface area between cracks	k_b	Number of dowels between cracks
		d_b (mm)	Dowel diameter

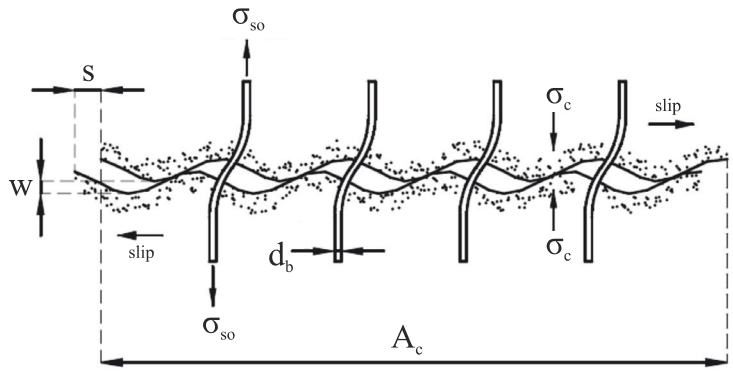

Figure 2.2. Interface dowel and friction mechanisms

A standard feature of any cyclic model is the envelope response curve, also known as 'skeleton curve', which is supplemented by the cyclic (hysteresis) rules. The envelope curves, according to Vassilopoulou and Tassios (2003), are defined by eqs. 2.1-2.2 for the dowel action D(s), and by 2.3-2.8 for the friction effect τ(s), respectively. The lower branch of eq. 2.1 may be implicitly solved by a root-finding method (e.g. Brent's). Equation notation can be referenced in Figure 2.2.

$$\begin{cases} D(s) = 0.5 \cdot D_u \cdot \dfrac{s}{s_{el}} & \text{for } \dfrac{D(s)}{D_u} \le 0.5 \\ s = 0.006 \cdot d_b + 1.76 \cdot 0.05 \cdot d_b \left[\left(\dfrac{D(s)}{D_u} \right)^4 - 0.50 \cdot \left(\dfrac{D(s)}{D_u} \right)^3 \right] & \text{for } \dfrac{D(s)}{D_u} > 0.5 \end{cases} \tag{2.1}$$

$$D_u = 1.3 \cdot d_b^2 \sqrt{f_y f_c} \tag{2.2}$$

$$\tau(s) = \begin{cases} 1.14 \cdot \tau_u(s) \cdot \left(\dfrac{s}{s_u} \right)^{1/3} & \text{for } \dfrac{s}{s_u} \le 0.5 \text{ , } s_u = 2 \text{ mm} \\ \tau_u(s) \cdot \left(0.81 + 0.19 \cdot \dfrac{s}{s_u} \right) & \text{for } \dfrac{s}{s_u} > 0.5 \text{ , } s_u = 2 \text{ mm} \\ \tau_u(s) & \text{for } \dfrac{s}{s_u} > 1.0 \text{ , } s_u = 2 \text{ mm} \end{cases} \tag{2.3}$$

$$\tau_u(s) = 0.44 \cdot \left[f_c^2 \sigma_c(s) \right]^{1/3} \tag{2.4}$$

$$\sigma_c(s) = \rho \cdot \sigma_{so}(s) \tag{2.5}$$

$$\rho = k_b \cdot \frac{\pi \cdot d_b^2}{4 \cdot A_c \cdot f_c} \tag{2.6}$$

$$\sigma_{so}(s) = \sqrt{\frac{w(s) \cdot E_s \cdot f_c}{2 \cdot d_b}} \tag{2.7}$$

$$w(s) = \begin{cases} 0.6 \cdot s^{2/3} & \text{for } s \le s_u \\ 0.6 \cdot s_u^{2/3} & \text{for } s > s_u \end{cases} \tag{2.8}$$

Due to the combined action of dowel and friction forces, the reinforcement axial capacity is considered to be 'consumed' by both mechanisms, according to the interaction equation 2.9. By solving this equation with respect to slip (s), a critical value s_{crit} is derived, which introduces the following interaction conditions in (a) dowel and (b) friction envelope curves:

(a) An upper bound value of dowel force $D(s_{crit})$ is imposed on the envelope curve, i.e. for slip values greater than s_{crit}, no further increase in the dowel force is allowed.
(b) In eq. 2.8, the ultimate slip value (s_u) is replaced with s_{crit}, i.e. for slip values greater than s_{crit}, no further increase in the crack opening w(s) is allowed.

$$\left(\frac{\sigma_{so}(s)}{f_y}\right)^{1.5} + \left(\frac{D(s)}{D_u}\right)^{1.5} = 1 \qquad (2.9)$$

Figure 2.3 shows worked examples of envelope curves with and without the interaction effect between dowel and friction actions. On these envelope curves, cyclic response rules are subsequently introduced. As noted earlier, the limitation of the original cyclic model by Vassilopoulou and Tassios (2003), which is based on previous studies by Vintzileou and Tassios (1987) and Tassios and Vintzileou (1987), is that the cyclic rules are covering only the special case of symmetric cyclic slip (i.e. cycling up to a constant slip value of $\pm s_n$). Figure 2.4 depicts the original cyclic rules which will be subsequently improved in order to handle arbitrary cyclic loading.

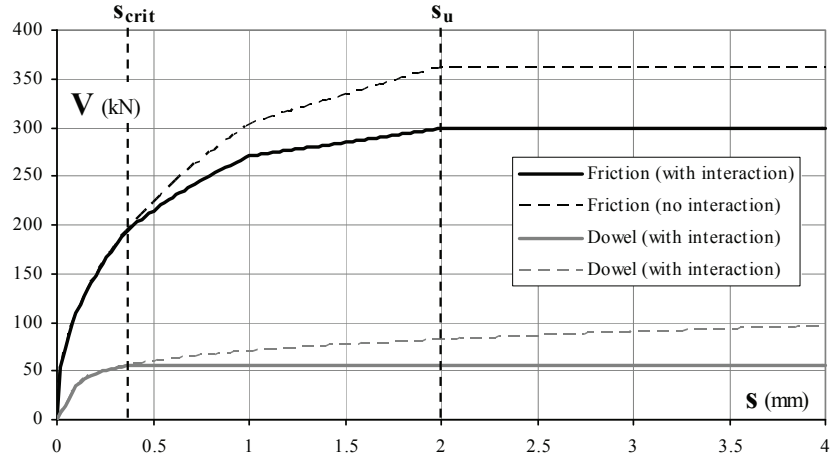

Figure 2.3. Dowel and friction envelope curves with and without interaction

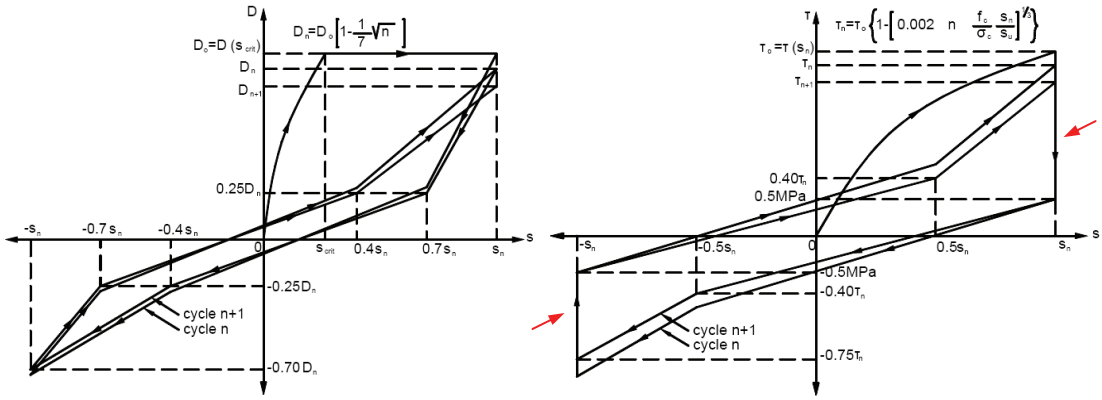

Figure 2.4. Symmetric dowel (left) and friction (right) cyclic response (Vassilopoulou and Tassios, 2003)

The new modifications in the above dowel and friction 'submodels' are described as follows:

- The envelopes, for positive slip values, follow equations 2.1 for dowel and 2.3 for friction forces, respectively. For negative slip values, these envelopes are reduced by 30 % and 25 % respectively (non-symmetrical).
- Since the dowel (D) and friction (τ) response shapes in Figure 2.4 are non-symmetrical, they are applicable only for an initial positive slip step. Consequently, if the initial step is negative, the

response shapes should be mirrored, hence a global 'direction' factor $\lambda = \text{sign}(s)$ is defined when the absolute current slip value exceeds the dowel elastic slip limit $s_{el} = 0.006 \cdot d_b$ for the first time.

- In the case of unloading or reloading from the envelope curve, the slip (s_r) and response (D_r or τ_r) are stored, at the moment of slip reversal. At the same moment, the absolute maximum recorded slip value (s_{max}) is also stored.
- Upon any slip reversal, the applicable range of the cyclic response is updated using eqs. 2.10-2.11 for dowel and 2.12-2.13 for friction forces. Figure 2.5 depicts the corresponding unloading and reloading paths the dowel submodel. In the special case when the starting (s_r) and ending (s_n) slip values are of the same sign, the depicted trilinear path is reduced to a straight line. Furthermore, in order to improve numerical stability, the vertical drops in friction force (arrows in Figure 2.4, right) were mitigated with a slip reduction of 10 %.

dowel range: $(s_r, D_r) \sim (s_n, D_n)$

unloading: $s_n = -s_{max}$ $\quad s_r > 0 : D_n = -0.7 \cdot |D_r|$ $\quad s_r < 0 : D_n = -|D_r|$ (2.10)

reloading: $s_n = s_{max}$ $\quad s_r > 0 : D_n = -|D_r|$ $\quad s_r < 0 : D_n = -|D_r| / 0.7$ (2.11)

friction range: $(s_r, \tau_r) \sim (s_n, \tau_n)$

unloading: $s_n = -s_{max}$ $\quad s_r > 0 : \tau_n = -0.75 \cdot |\tau_r|$ $\quad s_r < 0 : \tau_n = -|\tau_r|$ (2.12)

reloading: $s_n = s_{max}$ $\quad s_r > 0 : \tau_n = -|\tau_r|$ $\quad s_r < 0 : \tau_n = -|\tau_r| / 0.75$ (2.13)

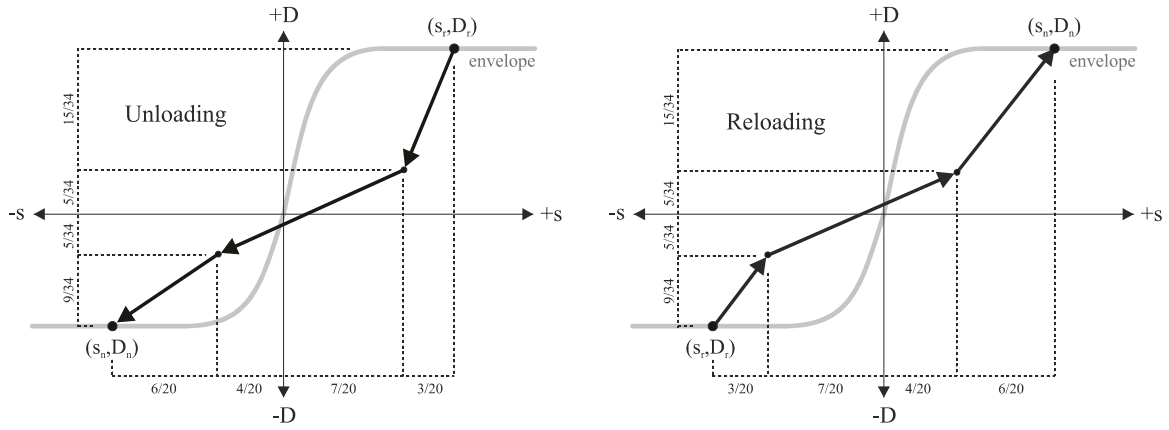

Figure 2.5. Unloading and reloading paths for dowel action

- If the ending slip value (s_n) is exceeded during loading (i.e. its absolute value is larger than s_{max}), the loading path continues on the envelope curve.
- In the case of $|s| < s_{el}$, elastic response is considered and no cyclic rules are applied.
- The final element of the improved cyclic interface model is the introduction of two force degradation factors for dowel and friction submodels. These degradation factors operate on the envelope curves and reflect the force degradation due to cyclic loading. In the original suggestion by Vassilopoulou and Tassios (2003) and in the later amendments of the Greek Code for Structural Interventions (KANEPE, 2012), the strength degradation depends on the number of symmetric cycles (n). In order to extend this concept to arbitrary loading history, an 'equivalent' number of cycles (n_{eq}) is introduced herein, depending on the cumulative slip (Σs):

$$n_{eq} = \frac{1}{4}\left(\frac{\sum s}{|s_{max}|} + 1 \right) \tag{2.14}$$

and the degradation factors for dowel (D_{deg}) and friction (τ_{deg}) actions are updated as follows:

$$D_{deg} = 1 - \frac{1}{7} \cdot \sqrt{n_{eq}} \tag{2.15}$$

$$\tau_{deg} = 1 - 0.05 \cdot \sqrt{n_{eq}} \sqrt{\frac{f_c}{\sigma_c}} \left(\frac{|s_{max}|}{s_u} \right)^{1/3} \tag{2.16}$$

The above degradation factors are pre-calculated at the moment of reloading yet finally applied on the envelope curves at the end of the cycling procedure, i.e. when the ending slip value (s_n) is exceeded and the loading path continues on an updated envelope curve. The transition between the former and the updated envelope is performed on the final branch of the cyclic load path, as depicted in Figure 2.6 for the dowel submodel.

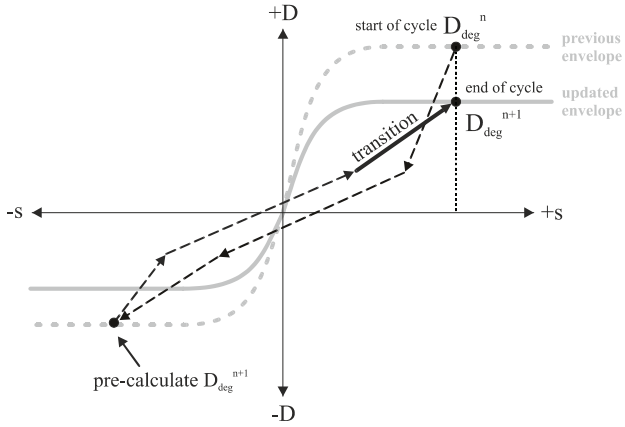

Figure 2.6. Calculation and update of the degradation factor and envelopes

- Finally, the total interface response from the combination of the dowel and friction submodels is calculated as follows:

$$V(s) = V_D(s) + V_F(s) = \lambda \cdot D(s) \cdot D_{deg} \cdot k_b + \lambda \cdot \tau(s) \cdot \tau_{deg} \cdot A_c \tag{2.17}$$

Figure 2.7 depicts worked examples of the interface model response, for symmetric, non-symmetric and arbitrary slip loading histories. It is observed that the suggested implementation exhibits numerical robustness and hence is deemed suitable for being integrated in the cyclic moment-curvature analysis solution strategy presented in the subsequent section.

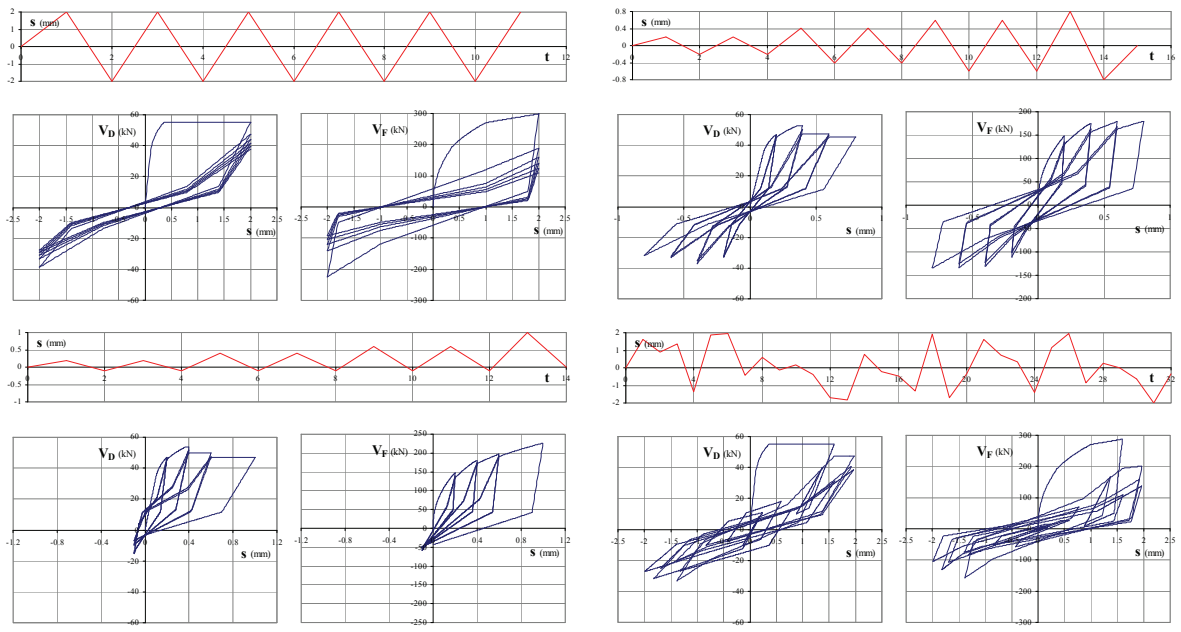

Figure 2.7. Interface response curves for various slip loading histories

3. SOLUTION STRATEGY

The computational procedure for the moment-curvature analysis of rectangular R/C jacketed sections, including interface slip, under cyclic loading, is based on the classic fiber decomposition approach due to the non-cylindrical stress field (non-uniform in one direction) emanating from the load path dependency which characterizes cyclic loading (Bonet et al., 2004). In this direction, the section is decomposed into a fine fiber mesh (Fig. 3.1, left) and each fiber is associated with the corresponding cyclic material constitutive model. It is noted here that three confinement regions are determined for the jacketed section (unconfined, partially confined, fully confined), each associated with a properly calculated confinement factor (see Tab. 2-1) according to the confinement model suggested by Kappos (1991). Furthermore, negative reinforcement fibers associated with the background concrete material are introduced at reinforcement locations, in order to account for the removed concrete area under reinforcement bars (Fafitis, 2001). For the stress integration of the section internal forces, following the Bernoulli-Euler assumption (i.e. plane sections remain plane and perpendicular to the axis of the column), the complete strain profile is described with four distinct parameters (φ, ε_o, ε_A, ε_B), in order to account for possible interface slip, as depicted in Figure 3.1 (right).

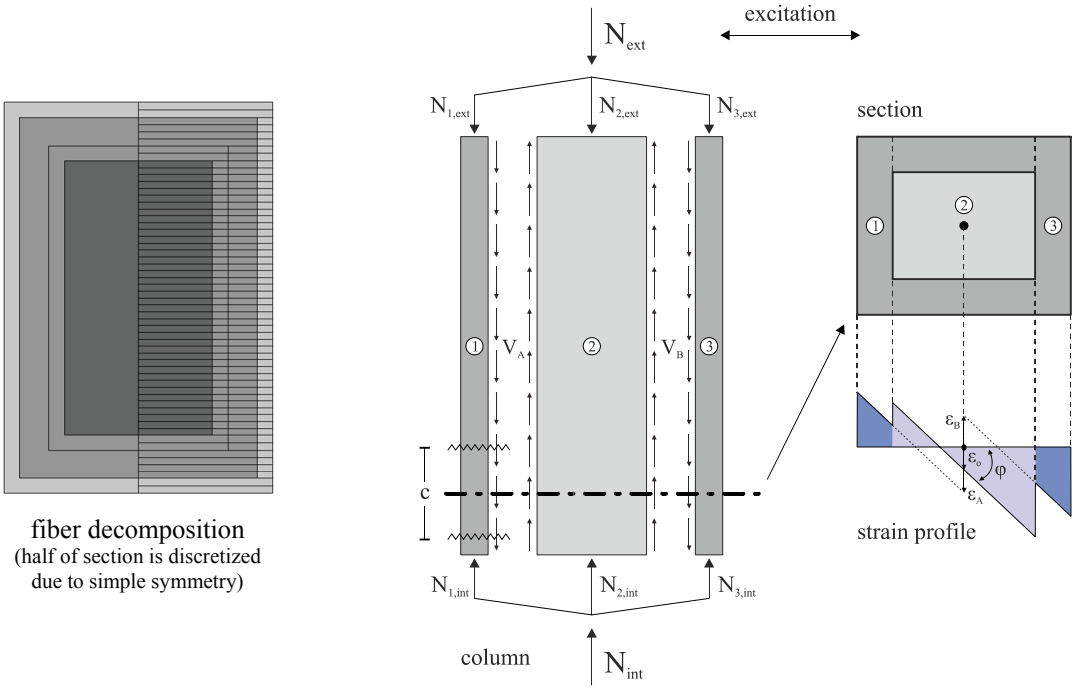

Figure 3.1. Section fiber decomposition (left), equilibrium conditions (center) and strain profile (right)

For each section fiber, the total strain is calculated according to its normal distance (y) from the section origin as follows:

$$\text{For } y < -h_c/2 \qquad \varepsilon = -\varphi \cdot y + \varepsilon_A \tag{3.1}$$

$$\text{For } -h_c/2 < y < h_c/2 \qquad \varepsilon = -\varphi \cdot y + \varepsilon_o \tag{3.2}$$

$$\text{For } y > h_c/2 \qquad \varepsilon = -\varphi \cdot y + \varepsilon_B \tag{3.3}$$

where h_c is the height of the core subsection. The above equations describe strains in total form, while the same equations are also applicable in incremental form. As a result, with the four strain profile parameters incremented, the updated fiber stress can be calculated as follows:

$$(\Delta\varphi, \Delta\varepsilon_o, \Delta\varepsilon_A, \Delta\varepsilon_B) \rightarrow \text{3.1-3.3} \rightarrow \text{fiber increment } \Delta\varepsilon \rightarrow \text{constitutive model} \rightarrow \text{fiber stress } (\sigma)$$

and finally, by integrating all fiber stresses, the total internal axial force (N_{int}) and moment (M) can be calculated as follows:

$$N_{int} = 2 \cdot \left(\sum_{i=1}^{Nc} \ell_{x,i} \cdot \ell_{y,i} \cdot \sigma_{c,i} + \sum_{i=1}^{Ns} \frac{\pi \cdot d_i^2}{4} \cdot \sigma_{s,i} - \sum_{i=1}^{Ns} \frac{\pi \cdot d_i^2}{4} \cdot \sigma_{c,i} \right) \quad (3.4)$$

$$M_{int} = 2 \cdot \left(\sum_{i=1}^{Nc} \ell_{x,i} \cdot \ell_{y,i} \cdot \sigma_{c,i} \cdot y_{c,i} + \sum_{i=1}^{Ns} \frac{\pi \cdot d_i^2}{4} \cdot \sigma_{s,i} \cdot y_{s,i} - \sum_{i=1}^{Ns} \frac{\pi \cdot d_i^2}{4} \cdot \sigma_{c,i} \cdot y_{s,i} \right) \quad (3.5)$$

where N is the number of fibers, ℓ_x and ℓ_y are the fiber dimensions, d is the rebar fiber diameter and indices c, s are for concrete and steel, respectively. In the same fashion, the internal axial forces of the three distinct zones (1-2-3 in Fig. 3.1, right), which are formed by the two interfaces are calculated and will be utilized below in the interface equilibrium conditions ($N_{int} = N_{1,int} + N_{2,int} + N_{3,int}$).

For simulating the interface slip between old and new concrete, two identical interface models are introduced which produce the shear forces V_A and V_B due to the relative slip (s_A and s_B) between the core and the jacket (Fig. 3.1, center). Furthermore the distance (c) between cracks in the direction of the column, where the interface model is considered to operate, is calculated by analytical expressions suggested in Thermou et al. (2004). The incremental change of the strain profile described above ($\Delta\varphi$, $\Delta\varepsilon_o$, $\Delta\varepsilon_A$, $\Delta\varepsilon_B$) causes slip in the top and bottom interface and modifies the corresponding shear forces as follows:

$$\Delta s_A = c \cdot (\Delta\varepsilon_A - \Delta\varepsilon_o) \rightarrow \text{interface model} \rightarrow \text{bottom interface shear } (V_A) \quad (3.6)$$

$$\Delta s_B = c \cdot (\Delta\varepsilon_B - \Delta\varepsilon_o) \rightarrow \text{interface model} \rightarrow \text{top interface shear } (V_B) \quad (3.7)$$

Finally, the global equilibrium conditions of the section are described as follows:

- Equilibrium of total axial force: $N_{int} = N_{ext}$ (3.8)
- Equilibrium of bottom interface: $V_A = N_{1,int} - N_{1,ext}$ (3.9)
- Equilibrium of top interface: $V_B = N_{3,int} - N_{3,ext}$ (3.10)

where $N_{1,ext}$ and $N_{3,ext}$ are calculated by the corresponding tributary areas in the case when the external axial load is applied to the entire section. If the external axial load is applied only on the core subsection (as in various experimental tests), the above values are zero. The aforementioned numerical procedures are summarized in Figure 3.2, where the nonlinear section equilibrium problem is described.

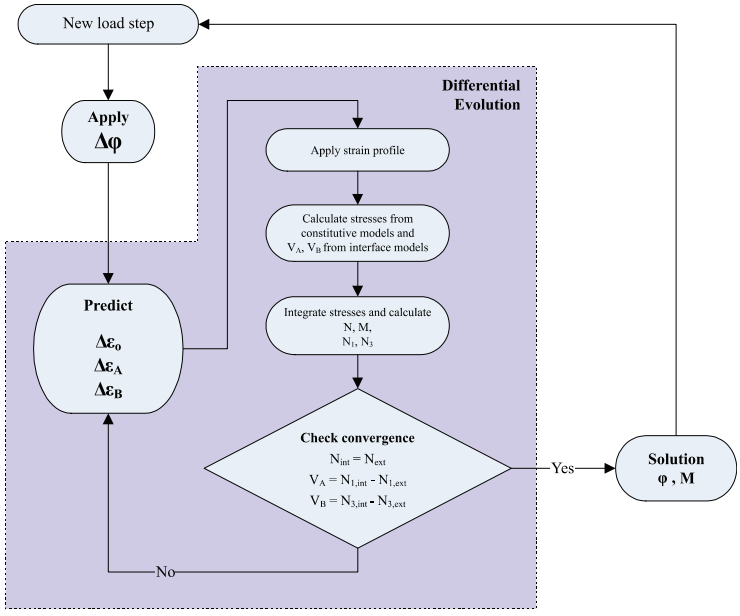

Figure 3.2. The nonlinear section equilibrium problem

According to Figure 3.2, for each curvature step ($\Delta\varphi$), the goal is to calculate the bending moment (M) corresponding to the new curvature value $\varphi+\Delta\varphi$, for a given constant external axial load (N_{ext}). This procedure is repeated for the entire curvature load history, in order to finally produce the requested cyclic moment-curvature response curve. For each (predefined) curvature step, in order to satisfy the aforementioned equilibrium conditions, the three unknowns ($\Delta\varepsilon_o$, $\Delta\varepsilon_A$, $\Delta\varepsilon_B$) which, together with $\Delta\varphi$, define the section strain profile should be determined. This kind of nonlinear problems can be traditionally solved by nested loops, seeking equilibrium by iterating each unknown separately. However, in the present case, this approach could lead to wrong estimates, considering the cyclic nature of the constitutive models; in Figure 3.3 (left), the interface model response for two different load paths (according to eq. 3.6), is depicted: (a) nested loop approach and (b) direct loading. In the first case, a slip of $c\cdot\Delta\varepsilon_A$ is applied in the inner loop until convergence and $-c\cdot\Delta\varepsilon_o$ in the outer. In the second case, slip loading is applied directly, i.e. $c\cdot\Delta\varepsilon_A - c\cdot\Delta\varepsilon_o = \Delta s_A$. It is apparent that the correct result corresponds to the second case because the cyclic model response is *load-path dependent*. Consequently, a 'trial-and-error' approach attempting different combinations of the three unknown values until convergence is required.

The nature of the aforementioned nonlinear problem hints to the application of an evolutionary algorithm, specifically the differential evolution approach (Storn and Price, 1997) which is an established metaheuristic method that optimizes a problem by iteratively improving a candidate solution (i.e. the present unknown set of $\Delta\varepsilon_o$, $\Delta\varepsilon_A$, $\Delta\varepsilon_B$) with regard to a given measure of quality, called the objective function. The main advantages of this method, whose details may be found in the original study by Storn and Price (1997), are its robustness and easy implementation. For the present problem the chosen parameters are the population NP = 30, weighting factor F = 0.5, crossover constant CR = 0.3, and the objective function is defined as follows:

$$f = \left|N_{int} - N_{ext}\right| + \left|N_{1,int} - N_{1,ext}\right| + \left|N_{3,int} - N_{3,ext}\right| \tag{3.11}$$

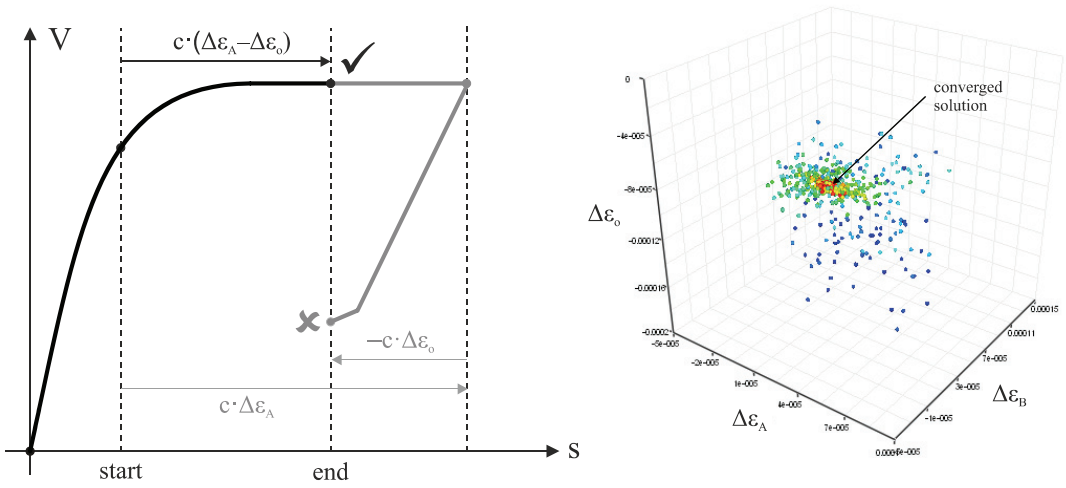

Figure 3.3. Interface response for sequential and direct slip loading (left) and convergence procedure of the differential evolution algorithm (right)

The above differential evolution algorithm, after a necessary number of objective function (eq. 3.11) evaluations yields the optimum solution vector $\mathbf{x} = [\Delta\varepsilon_o, \Delta\varepsilon_A, \Delta\varepsilon_B]^T$, providing that $f < 10^{-4}$ (tolerance). Figure 3.3 (right) shows a 3D plot of trial solution vectors for a single curvature load step ($\Delta\varphi$). The vector color (blue to red) shows the continuous optimization of the solution towards convergence. Finally, a worked example of a jacketed R/C column under cyclic curvature loading, with and without consideration of interface slip is depicted in Figure 3.4, which demonstrates the efficiency of the suggested approach. It is observed that the introduction of interface slip results to a softened post-peak response due to the continuous deterioration of the interface between the core and the jacket. A more rigorous parametric evaluation of the present analytical method can be found in Thermou et al. (2012).

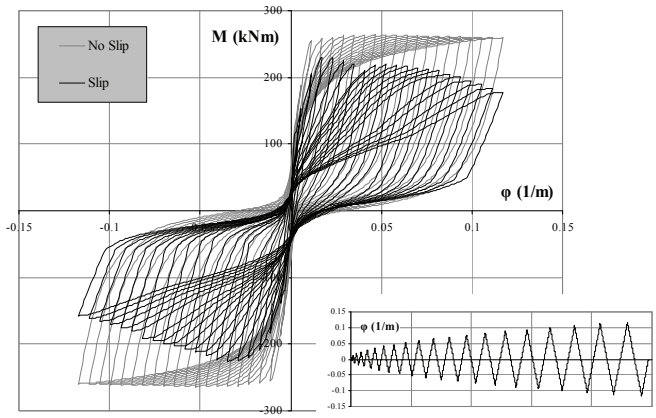

Figure 3.4. Moment-curvature response of a jacketed R/C column with and without considering interface slip

4. CLOSURE

A new analytical procedure was presented for the moment curvature analysis of jacketed R/C sections under cyclic loading, including interface slip. The included novelties are the improved cyclic interface model and the application of an evolutionary algorithm on cyclic moment-curvature section analysis. The computational robustness of the suggested method was validated with worked examples on constitutive and section level. It is believed that the present study contributes to the current state of knowledge on a subject of practical relevance, open to further investigations.

ACKNOWLEDGEMENT

The research reported herein was funded by the Hellenic Earthquake Planning and Protection Organization (EPPO); this support is gratefully acknowledged.

REFERENCES

Bonet, J.L., Romero, M.L., Miguel, P.F. and Fernandez, M.A. (2004). A fast stress integration algorithm for reinforced concrete sections with axial loads and biaxial bending. Computers & Structures **82:2-3**, 213-225.

Elnashai, A.S., Papanikolaou, V.K., and Lee, D.H. (2010). Zeus-NL – A program for inelastic dynamic analysis of structures. *Mid-America Earthquake Center*, University of Illinois at Urbana Champaign, USA.

Fafitis, A. (2001). Interaction surfaces of reinforced concrete sections in biaxial bending. *Journal of Structural Engineering, ASCE* **127:7**, pp. 840-846.

Filippou, F.C., Popov, E.P. and Bertero, V.V. (1983). Effects of bond deterioration on hysteretic behaviour of reinforced concrete joints. *Report No. UCB/EERC-83/19*, University of California, Berkeley.

KANEPE (2012). Greek Code for Structural Interventions. *Earthquake Planning and Protection Organization (EPPO)*, Athens, Greece.

Kappos, A.J. (1991). Analytical prediction of the collapse earthquake for R/C buildings : Suggested methodology. *Earthquake Engineering and Structural Dynamics* **20:2**, 167-176.

Mander J.B., Priestley M.J.N. and Park R. (1988). Theoretical stress-strain model for confined concrete. *Journal of Structural Engineering* **114:8**, 1804-1826.

Martinez-Rueda J.E. and Elnashai A.S. (1997). Confined concrete model under cyclic load. *Materials and Structures* **30:3**, 139-147.

Menegotto, M. and Pinto, P.E (1973). Method of analysis for cyclically loaded RC plane frames including changes in geometry and nonelastic behaviour of elements under combined normal force and bending. *Proc. IABSE Symposium*, Lisbon, Portugal.

Storn, R. and Price, K. (1997). Differential Evolution – A simple and efficient heuristic for global optimization over continuous spaces, *Journal of Global Optimization* **11:4**, 341-359.

Tassios, T.P. and Vintzileou, E. (1987). Concrete to concrete friction. *Journal of Struct. Engineering, ASCE* **113:4**, 832-849.

Thermou, G. E., Pantazopoulou, S. J., and Elnashai, A. S. (2004). Analytical modeling of interface behavior in reinforced concrete jacketed members." *Proc. Structures Congress (ASCE)*, No. 349, Nashville, Tennessee, USA.

Thermou, G.E., Papanikolaou, V.K. and Kappos, A.J. (2012). Cyclic Response of R/C Jacketed Columns Including Modelling of the Interface Behaviour. *15th World Conference on Earthquake Engineering*, Lisbon, Portugal.

Vassilopoulou, I. and Tassios, P. (2003). Shear transfer capacity along a RC crack under cyclic sliding. *Proc. fib Symposium*, No. 271, Technical Chamber of Greece, Athens, Greece.

Vintzileou, E. and Tassios, T.P. (1987). Behaviour of dowels under cyclic deformations. *ACI Structural Journal* **84:1**, 18-30.